Grown-in Defects of InSb Crystals: Models and Computation

N. Vaidya [*], H. Huang [†] and D. Liang [‡]
Department of Mathematics & Statistics, York University
Toronto, Canada M3J 1P3.

August 22, 2005

Abstract

In this paper, we present a model for grown-in point defects inside indium antimonide crystals grown by the Czochralski technique. Our model is similar to the ones used for silicon crystal, which includes the Fickian diffusion and a recombination mechanism. This type of models is used for the first time to analyze grown-in point defects in indium antimonide crystals.

The temperature solution and the advance of the melt-crystal interface, which determines the time-dependent domain of the model, are based on a recently derived perturbation model. We propose a finite difference method which takes into account of the moving interface. We study the effect of thermal flux on the point defect patterns during and at the end of the growth process. Our results show that the concentration of excessive point defects is positively correlated to the heat flux in the system.

Keywords: Crystal growth; Czochralski Technique; Point defects; Recombination; Thermal flux; Finite difference method.

1 Introduction

Indium antimonide (InSb), a compound semiconductor which is useful as an infrared detector and filter, has attracted considerable attention over the last several years. Due to thermal fluctuation and/or presence of impurities during the crystal growth process, the structure of the crystal posses various imperfections, known as defects. Among various types of defect, the basic ones are the point defects (interstitial, vacancy, interstitialcy).

[*] nvaidya@mathstat.yorku.ca
[†] hhuang@yorku.ca
[‡] dliang@mathstat.yorku.ca

Most of the previous work on point defects has been done for silicon crystals. Taking convective flux, diffusive flux and recombination of interstitials and vacancies into account, Voronkov [21, 22] proposed a model of micro-defect formation in silicon and authers in [8, 13, 14, 15] followed the similar models. While many researchers [4, 5, 11, 12, 18] have improved the model by adding the reduced heat transfer effects Sinno et al [17] has further added the effect of nucleation of excess vacancies or excess interstitials. While the general principle is similar for different types of crystals, material properties may have an impact on the formation and dynamics of point defects.

In this paper we extend the Voronkov model [22] to indium antimonide crystal grown by the CZ technique. The main objective of the paper is to compute the distribution of point defects and their supersaturation values by solving the model equations numerically. We will exam the effect of controlling parameters such as the heat fluxes at the gas/crystal and melt/crystal interfaces on the point defects distribution. The rest of the paper proceeds as follows. We present our basic model for two types of point defects in Section 2. A numerical method for solving the model equations is proposed in Section 3. Numerical results for the basic model is given in Section 4 and we finish the paper by a short discussion in Section 5. A generalization of the basic model is given in the Appendix.

2 Basic Model

To simplify the computation, we neglect the impurity atom and interstitialcy defects. Furthermore, we consider only neutral species of point defects and neglect charged species and focus on the distribution of two types of point defects, namely interstitial and vacancy. Taking convective flux, diffusive flux as a Fickian diffusion and recombination reaction between interstitial and vacancy into account, mathematical model governing the point defects is of the reaction-diffusion type, written as

$$\frac{\partial C_I}{\partial t} = \nabla \cdot (D_I \nabla C_I - \vec{f}_p C_I) - R_{IV}(C_I C_V - C_I^e C_V^e), \tag{1}$$

$$\frac{\partial C_V}{\partial t} = \nabla \cdot (D_V \nabla C_V - \vec{f}_p C_V) - R_{IV}(C_I C_V - C_I^e C_V^e), \tag{2}$$

where C_I and C_V are volume concentrations of interstitial and vacancy point defects, respectively. R_{IV} is the temperature dependent reaction rate, which determines how fast the recombination is taking place. It can be expressed as a function of the mobility of point defects and a free energy activation barrier as

$$R_{IV} = 4\pi a_r (D_I(T) + D_V(T)) e^{-\frac{\Delta G_{IV}}{k_B T}},$$

where a_r is an effective capture radius, k_B, the Boltzmann's constant and ΔG_{IV}, the free energy barrier against recombination of interstitial and vacancy. C_j^e, $j = I, V$ are the equilibria of C_j for a given temperature T, given by the formula

$$C_j^e = C_j^0 e^{-\frac{E_{jf}}{k_B}\left(\frac{1}{T} - \frac{1}{T_0}\right)}$$

where C_j^0 is the value at reference temperature T_0, the melting temperature and E_{jf}, the formation energy of j-type defect. The diffusion coefficient $D_j(T)$ is given by the formula

$$D_j(T) = D_j^0 e^{-\frac{E_j}{k_B T}}$$

where D_j^0 is the pre-exponential constant and E_j, the activation energy for diffusion of the j-type point defect.

Now, the coordinate system is fixed at the top of the crystal. Then $\vec{f_p}$ is the interface speed due to growth and we have fixed our coordinate on the moving melt-solid interface. Assuming that the growth direction is in the $z-$direction, one-dimensional model equations can be rewritten as

$$\frac{\partial C_I}{\partial t} = \frac{\partial}{\partial z}\left(D_I \frac{\partial C_I}{\partial z}\right) - R_{IV}(C_I C_V - C_I^e C_V^e), \tag{3}$$

$$\frac{\partial C_V}{\partial t} = \frac{\partial}{\partial z}\left(D_V \frac{\partial C_V}{\partial z}\right) - R_{IV}(C_I C_V - C_I^e C_V^e), \tag{4}$$

for $0 \leq z \leq S(t)$ where S(t) is the position of melt/crystal interface.

At the interface ($z = S(t)$) defects are formed and their values are assumed to be the equilibria values. At the top ($z = 0$) we assume that the flux of the defects are zero. Therefore, to solve the one dimensional model equations, we apply the following boundary conditions:

$$\begin{array}{rrl} \text{[interface]} & z = S(t): & C_j = C_j^0, \\ \text{[top]} & z = 0: & \frac{\partial C_j}{\partial z} = 0. \end{array} \tag{5}$$

Higher dimensional models can be constructed similarly. In this paper, we consider a perfectly cylindrical axi-symmetric crystal. As in the one-dimensional case, the two-dimensional model equations are

$$\frac{\partial C_I}{\partial t} = \frac{\partial}{\partial z}\left(D_I \frac{\partial C_I}{\partial z}\right) + \frac{1}{r}\frac{\partial}{\partial r}\left(r D_I \frac{\partial C_I}{\partial r}\right) - R_{IV}(C_I C_V - C_I^e C_V^e), \tag{6}$$

$$\frac{\partial C_V}{\partial t} = \frac{\partial}{\partial z}\left(D_V \frac{\partial C_V}{\partial z}\right) + \frac{1}{r}\frac{\partial}{\partial r}\left(r D_V \frac{\partial C_V}{\partial r}\right) - R_{IV}(C_I C_V - C_I^e C_V^e), \tag{7}$$

for $0 \leq r \leq R$ where R is the radius of the cylindrical crystal.

Imposing no flux condition at the lateral surface in contact with gas ($r = R$) and symmetric condition at the center of the crystal ($r = 0$), we get the following boundary conditions in the case of axi-symmetric cylindrical crystal:

$$\begin{array}{rrl} \text{[interface]} & z = S(t): & C_j = C_j^0, \\ \text{[top]} & z = 0: & \frac{\partial C_j}{\partial z} = 0, \\ \text{[center]} & r = 0: & \frac{\partial C_j}{\partial r} = 0, \\ \text{[lateral surface]} & r = R: & \frac{\partial C_j}{\partial r} = 0. \end{array} \tag{8}$$

The diffusion coefficient D_j, the equilibrium concentration C_j^e and the rate of recombination reaction R_{IV} are all functions of temperature. So, the temperature distribution inside the crystal plays a major role in the distribution of point defects. The dynamics of the temperature profile T inside the crystal is governed by the heat equation

$$\rho_s c_s \frac{\partial T}{\partial t} = k_s \nabla^2 T, \tag{9}$$

where ρ_s, c_s and k_s are the density, specific heat capacity and the thermal conductivity of the crystal respectively. The temperature at the crystal-melt interface boundary is fixed as the melting temperature T_0 and Newton's cooling law is applied at other boundaries i.e. at the lateral surface and at the top of the crystal. Therefore, for solving equation (9), following boundary conditions can be used:

$$\begin{aligned} \text{[interface]}: &\quad T = T_0, \\ \text{[lateral surface]}: &\quad -k_s \tfrac{\partial T}{\partial n} = h_{gs}(T - T_g), \\ \text{[top]}: &\quad k_s \tfrac{\partial T}{\partial z} = h_{ch}(T - T_{ch}) \end{aligned} \tag{10}$$

where $\vec{n}$, T_g, h_{gs} and h_{ch} are outward unit normal vector, ambient gas temperature, crystal-gas heat transfer coefficient and seed-chuck heat transfer coefficient respectively. The interface position $z = S(r, t)$ of the growing crystal, which determines the domain of the point-defects model equations, can be obtained by the help of the Stefan condition

$$\rho_s L \frac{\partial S}{\partial t} = k_s \left. \frac{\partial T}{\partial n} \right|_{z \to S^-} - q_l \tag{11}$$

where L and q_l are the latent heat and the heat flux from the melt respectively.

We normalize the concentration with respective to C_I^0 and let

$$u = \frac{C_I}{C_I^0}, \; v = \frac{C_V}{C_I^0}, \; \hat{t} = t^* t, \text{with } t^* = 4\pi a_r C_I^0 D_I^0 e^{-\frac{E_I + \Delta G_{IV}}{k_B T_0}}$$

and dropping the hat we get the resulting equations for u and v as follows:

$$\frac{\partial u}{\partial t} = D_I^* \frac{\partial}{\partial z} \left(\overline{D}_I \frac{\partial u}{\partial z} \right) - \overline{R}_{IV}(uv - u^e v^e) \tag{12}$$

$$\frac{\partial v}{\partial t} = D_v^* \frac{\partial}{\partial z} \left(\overline{D}_v \frac{\partial v}{\partial z} \right) - \overline{R}_{IV}(uv - u^e v^e) \tag{13}$$

where

$$D_I^* = \frac{1}{4\pi a_r C_I^0 e^{-\frac{\Delta G_{IV}}{k_B T_0}}}, D_V^* = \frac{D_V^0 D_I^*}{D_I^0},$$

$$\overline{D}_I(T) = e^{-\frac{E_I}{k_B}\left(\frac{1}{T} - \frac{1}{T_0}\right)}, \overline{D}_V(T) = e^{-\frac{1}{k_B}\left(\frac{E_V}{T} - \frac{E_I}{T_0}\right)},$$

$$\overline{R}_{IV}(T) = e^{-\frac{\Delta G_{IV}}{k_B}\left(\frac{1}{T}-\frac{1}{T_0}\right)}\left(e^{-\frac{E_I}{k_B}\left(\frac{1}{T}-\frac{1}{T_0}\right)} + \frac{D_V^0}{D_I^0}e^{-\frac{1}{k_B}\left(\frac{E_V}{T}-\frac{E_I}{T_0}\right)}\right),$$

$$u^e = \frac{C_I^e}{C_I^0}, v^e = \frac{C_V^e}{C_I^0}.$$

Similarly, the two-dimensional equations for u and v are as follows:

$$\frac{\partial u}{\partial t} = D_I^* \frac{\partial}{\partial z}\left(\overline{D}_I \frac{\partial u}{\partial z}\right) + \frac{D_I^*}{r}\frac{\partial}{\partial r}\left(r\overline{D}_I\frac{\partial u}{\partial r}\right) - \overline{R}_{IV}(uv - u^e v^e), \tag{14}$$

$$\frac{\partial v}{\partial t} = D_v^* \frac{\partial}{\partial z}\left(\overline{D}_v \frac{\partial v}{\partial z}\right) + \frac{D_V^*}{r}\frac{\partial}{\partial r}\left(r\overline{D}_V\frac{\partial v}{\partial r}\right) - \overline{R}_{IV}(uv - u^e v^e). \tag{15}$$

In order to compute the distribution of the point defects, we have to solve the coupled system of point defects model equations as well as the temperature equation. Since an approximate solution is available for temperature, for simplicity, we will use the temperature solution obtained in [1], which is reproduced below. For the one-dimensional case, we have

$$T(z,t) = T_g + (T_0 - T_g)\Theta_0(\hat{z},\hat{t}), \tag{16}$$

with

$$\Theta_0(\hat{z},\hat{t}) = \frac{\sqrt{2}\cosh\sqrt{2}\hat{z} + \delta\sinh\sqrt{2}\hat{z} + \delta\Theta_{ch}\sinh\sqrt{2}(S_0(\hat{t}) - \hat{z})}{\sqrt{2}\cosh\sqrt{2}S_0(\hat{t}) + \delta\sinh\sqrt{2}S_0(\hat{t})}, \tag{17}$$

$$\frac{dS_0(\hat{t})}{d\hat{t}} = \sqrt{2}\frac{\sqrt{2}\sinh\sqrt{2}S_0(\hat{t}) + \delta\cosh\sqrt{2}S_0(\hat{t}) - \delta\Theta_{ch}}{\sqrt{2}\cosh\sqrt{2}S_0(\hat{t}) + \delta\sinh\sqrt{2}S_0(\hat{t})} - \gamma \tag{18}$$

where $S_0(0) = \frac{\sqrt{\epsilon}}{R}Z_{\text{seed}}$, $S_0(\hat{t}) = \frac{\sqrt{\epsilon}}{R}S(t)$, $\hat{z} = \frac{\sqrt{\epsilon}}{R}z$, $\epsilon = \frac{h_{gs}R}{k_s}$, $\gamma = \frac{q_l R}{\epsilon^{1/2}k_s.(T_0-T_g)}$, $\delta = \epsilon^{1/2}h_{ch}/h_{gs}$, $\hat{t} = \frac{k_s\epsilon(T_0-T_g)}{LR^2\rho_s}t$. The values $\delta = 0$ and $\Theta_{ch} = 0$ correspond to the insulated chuck and the cold chuck respectively. Here, Z_{seed} denotes the length of the seed crystal.

Similarly, for the two-dimensional model, the temperature distribution inside the cylindrical crystal has been given in [1] as

$$T(r,z,t) = T_g + (T_0 - T_g)\left(\left(1 - \frac{\epsilon\hat{r}^2}{2}\right)\Theta_0(\hat{z},\hat{t}) + \epsilon\Theta_1^0(\hat{z},\hat{t})\right), \tag{19}$$

$$\Theta_1^0(\hat{z},\hat{t}) = \frac{1}{4\sqrt{2}}\frac{\cosh\sqrt{2}\hat{z}}{\cosh\sqrt{2}S_0}(S_0\tanh\sqrt{2}S_0 - \hat{z}\tanh\sqrt{2}\hat{z} - 8S_1^0\tanh\sqrt{2}S_0) \tag{20}$$

where $\hat{r} = \frac{r}{R}$.

3 Solution Methodology

We solve the one-dimensional as well as the two-dimensional equations by numerical method. To solve these systems of partial differential equations, we use the finite dfference method.

As the boundary is moving (i.e. the crystal is growing) the size of the domain is increasing with time. So, we have to update the domain at each time-step by using the ordinary differential equation (18). This will determine the temperature profile too. Therefore, while solving the system, we are not only solving for the concentration density of point defects but also solving for the temperature distribution. Since the rate of the advance of the interface is not constant, if we expect to keep uniform spatial step-size, we might end up geting grid points different from those in the previous time-step. The value of these new grid points can be calculated by using some interpolation techniques. However, we are not following this technique here. We will work with the non-uniform spatial step-size. Keeping the previous grids as they are, we add the boundary point (interface) of the previous time-step as a new grid point and the present interface position is taken as a new boundary. But in this method, we have to be careful to choose the time-step because the time-step will determine the added spatial step-size. In fact, the time-step should be chosen sufficiently small so that the length of the advance of the interface is comparable with the existing spatial step-size. At the boundaries in which Neumann's boundary conditions are given, we determine numerically the boundary values by using Taylor expansion with the given boundary conditions.

3.1 One-dimensional case

We propose the following numerical scheme for solving the one-dimensional equations (12) and (13).

Let the temporal step-size be Δt, chosen sufficiently small. Let $0 = z_0 < z_1 < ...... < z_N = N\Delta t$ be a partition of $[0, S(t)] = [0, N\Delta t]$ at the Nth time-step and $u_l, v_l, l = 1, 2, ..., N-1$ be approximations to u, v respectively at the grid point z_l. On a non-uniform mesh grid, we use the following discretization.

$$\frac{\partial}{\partial z}\left(\overline{D}_I \frac{\partial u}{\partial z}\right)\Bigg|_{z_l} = \frac{2}{z_{l+1} - z_l}\left(\overline{D}_I(T(z_{l+\frac{1}{2}}))\frac{u_{l+1} - u_l}{z_{l+1} - z_l} - \overline{D}_I(T(z_{l-\frac{1}{2}}))\frac{u_l - u_{l-1}}{z_l - z_{l-1}}\right).$$

The diffusion term in v-equation is done in the same way.

We use the implicit method of discretization for the diffusion term and the non-linear source term will be handled explicitely. After making the approximate solutions u_l and v_l to satisfy equations (12) and (13), we obtain the following scheme

$$\begin{aligned} -A^{l,u}_{l-1} u^{n+1}_{l-1} + A^{l,u}_{l} u^{n+1}_{l} - A^{l,u}_{l+1} u^{n+1}_{l+1} &= u^n_l - \Delta t \alpha^n_l \\ -A^{l,v}_{l-1} v^{n+1}_{l-1} + A^{l,v}_{l} v^{n+1}_{l} - A^{l,v}_{l+1} v^{n+1}_{l+1} &= v^n_l - \Delta t \alpha^n_l, \\ l = 1, 2, ...N-1. \end{aligned} \tag{21}$$

where

$$A^{l,j}_{l-1} = \frac{2\Delta t D^*_J \overline{D}_J(T(z_{l-\frac{1}{2}}))}{(z_{l+1} - z_{l-1})(z_l - z_{l-1})},$$

$$
\begin{aligned}
A_l^{l,j} &= 1 + \frac{2\Delta t D_J^*}{z_{l+1} - z_{l-1}} \left(\frac{\overline{D}_J(T(z_{l+\frac{1}{2}}))}{z_{l+1} - z_l} + \frac{\overline{D}_J(T(z_{l-\frac{1}{2}}))}{z_l - z_{l-1}} \right), \\
A_{l+1}^{l,j} &= \frac{2\Delta t D_J^* \overline{D}_J(T(z_{l+\frac{1}{2}}))}{(z_{l+1} - z_{l-1})(z_{l+1} - z_l)}, \\
\alpha_l^n &= \overline{R}_{IV}(T(z_l))(u_l^n v_l^n - u^e(T(z_l))v^e(T(z_l))), \\
j &= u, v \text{ for corresponding } \mathrm{J} = \mathrm{I}, \mathrm{V} \text{ respectively.}
\end{aligned}
$$

3.2 Two-dimensional case

Similarly, we propose the following numerical scheme for solving the two-dimensional equations (14) and (15).

We keep the temporal step-size and the partition along the z-direction (growth direction) same as those in the one-dimensional case. We set $\Delta r = \frac{R}{N_r}$ as the spatial step-size in the radial direction. Let $u^{l,m}, v^{l,m}; l = 1, 2, ..., N-1; m = 1, 2, ..., N_r - 1$ be approximations to u, v respectively at the grid point $(z_l, r_m = m\Delta r)$. The approximate solutions are made to satisfy the equations (14) and (15) at each grid point. This produces the following scheme:

$$
\begin{aligned}
-A_{l-1,m}^{lm,u} u_{l-1,m}^{n+1} - A_{l,m-1}^{lm,u} u_{l,m-1}^{n+1} + A_{l,m}^{lm,u} u_{l,m}^{n+1} - A_{l,m+1}^{lm,u} u_{l,m+1}^{n+1} - A_{l+1,m}^{lm,u} u_{l+1,m}^{n+1} &= u_{l,m}^n - \alpha_{l,m}^n \\
-A_{l-1,m}^{lm,v} v_{l-1,m}^{n+1} - A_{l,m-1}^{lm,v} v_{l,m-1}^{n+1} + A_{l,m}^{lm,v} v_{l,m}^{n+1} - A_{l,m+1}^{lm,v} v_{l,m+1}^{n+1} - A_{l+1,m}^{lm,v} v_{l+1,m}^{n+1} &= v_{l,m}^n - \alpha_{l,m}^n, \\
l = 1, 2, ..., N-1; m = 1, 2, ..., N_r - 1. & \qquad (22)
\end{aligned}
$$

where,

$$
\begin{aligned}
A_{l-1,m}^{lm,j} &= \frac{2\Delta t D_J^* \overline{D}_J(T(z_{l-\frac{1}{2}}, r_m))}{(z_{l+1} - z_{l-1})(z_l - z_{l-1})}, \\
A_{l,m-1}^{lm,j} &= \frac{\Delta t D_J^* r_{m-\frac{1}{2}} \overline{D}_J(T(z_l, r_{m-\frac{1}{2}}))}{r_m \Delta r^2}, \\
A_{l,m}^{lm,j} &= 1 + \Delta t D_J^* \left[\frac{2}{z_{l+1} - z_{l-1}} \left(\frac{\overline{D}_J(T(z_{l+\frac{1}{2}}, r_m))}{z_{l+1} - z_l} + \frac{\overline{D}_J(T(z_{l-\frac{1}{2}}, r_m))}{z_l - z_{l-1}} \right) \right. \\
&\quad \left. + \frac{1}{r_m \Delta r^2} \left(r_{m+\frac{1}{2}} \overline{D}_J(T(z_l, r_{m+\frac{1}{2}})) + r_{m-\frac{1}{2}} \overline{D}_J(T(z_l, r_{m-\frac{1}{2}})) \right) \right], \\
A_{l,m+1}^{lm,j} &= \frac{\Delta t D_J^* \overline{D}_J(T(z_l, r_{m+\frac{1}{2}}))}{r_m \Delta r^2}, \\
A_{l+1,m}^{lm,j} &= \frac{2\Delta t D_J^* \overline{D}_J(T(z_{l+\frac{1}{2}}, r_m))}{(z_{l+1} - z_{l-1})(z_{l+1} - z_l)}, \\
\alpha_{l,m}^n &= \Delta t \overline{R}_{IV}(T(z_l, r_m))(u_{l,m}^n v_{l,m}^n - u^e(T(z_l, r_m))v^e(T(z_l, r_m))), \\
j &= u, v \text{ for corresponsing } \mathrm{J} = \mathrm{I}, \mathrm{V} \text{ respectively.}
\end{aligned}
$$

For each time step, the interface position is determined by solving equation (18) using Euler's method. In the case of two-dimensional scheme, the system of equations is solved by

Table 1: *Outline of the numerical algorithm*

	Initial variables
1.	Set a partition of initial crystal (seed) (which can be taken as uniform mesh).
2.	Determine Δt sufficiently small so that added spatial step-size is comparable with the existing step-size.
3.	Advance the interface by solving equation (18).
4.	Update the partition by adding previous boundary (interface) point as an interior grid and new interface position as a boundary.
5.	Solve the sustem of equations (21) in 1-dimensional case and (22) in 2-dimensinal case.
6.	STOP if the crystal is reached the desired length otherwise go to step 3.

Jacobi iteration method. Use of Jacobi iteration method makes this scheme suitable also for the parallel computaion. A brief overview of the computation has been outlined in Table 1. The values of the parameters used during calculation are given in Table 2 and Table 3. The free energy barrier for recombination is taken as the difference between the formation energies of corresponding interstitial and vacancy.

4 Results and Discussion

4.1 One-dimensional case

4.1.1 Point defects concentration

Since terms in the model are temperature-dependent, in the distribution of point defects inside the crystal, the distribution and variation of temperature inside the crystal play the most important role. In fact, the length of the crystal continues to increase as time passes. The length of the crystal reached during growth at different times is shown in Fig. 1(a). The length calculated here is for 28 hours of growth. This length depends upon the value of γ and the value of h_{gs} used. Increasing the value of γ decreases the length of the crystal whereas increasing the value of h_{gs} increases the length of the crystal in a particular duration of growth. The case shown here is for $\gamma = 0$, h_{gs}=3 W/m^{2}K and $R = 0.045m$. At the end of 28 hours, the growth of this condition will result in a crystal of length 30.11 cm. On average, it grows by 10.75 mm/hr, which is slower than the normally adopted value in practice.

Temperature is time- as well as space-dependent. The temperature distribution inside the crystal reached at different lengths at different times during the growth has been presented in Fig. 1(b). Temperature at the interface is always melting temperature. At the beginning the temperature remains nearly the same because the crystal length is very small, which is the length of the seed. Finally there is a rapid drop of the temperature from the interface to the top.

Table 2: *Parameter values for InSb Crystal (Source: [7]).*

Item	Symbol	Value
Equilibrium concentration at melting point (m^{-3})		
Interstitial	C_I^0	1.12×10^{20}
Vacancy	C_V^0	1.2×10^{20}
Pre-exponential factor for diffusion (m^2/s)		
Interstitial	D_I^0	1.76×10^9
Vacancy	D_V^0	1×10^8
Formation energy (eV)		
Interstitial	E_{If}	3.2
Vacancy	E_{Vf}	1.76
Activation energy for diffusion (eV)		
Interstitial	E_I	4.3
Vacancy	E_V	3.2
Free energy barrier against recombination(eV)		
Interstitial + Vacancy	G_{IV}	1.44
Effective capture radius for recombination (m)		
Interstitial + Vacancy	a_r	10^{-12}

Table 3: *Additional parameter values for InSb Crystal (Source: [1]).*

Item	Symbol	Value
Melt temperature	T_0	798 K
Pulling speed	f_p	6.944×10^{-6} m/s
Mean crystal radius	Rm	0.045 m
Final crystal length	Z	$0.30 - 0.34$ m
Ambient gas temperature	T_g	600 K
Solidus temperature	T_s	798.4 K
Density	ρ_s	5.64×10^3 kg/m^3
Thermal conductivity	k_s	4.57 W/m K
Heat capacity	$\rho_s c_s$	1.5×10^6 J/m^3 K
Latent heat of fusion	L	2.3×10^5 J/kg
Crystal-Gas heat transfer coefficient	h_{gs}	$1 - 4$ W/m^2 K
Boltzman's constant	k	$1.38 \times 10^{-23} JK^{-1}$

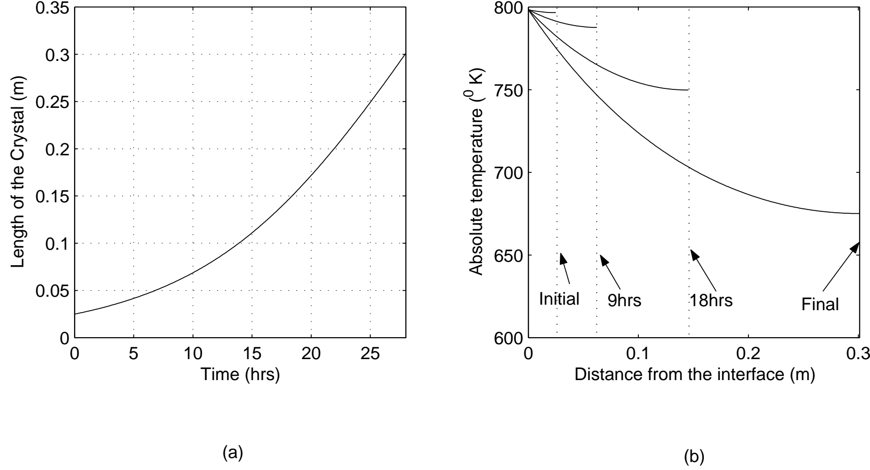

Figure 1: (a) Length of the crystal reached at different instant during 28 hours growth with $\gamma = 0$ and $h_{gs} = 3$ W/m^{2}K. (b) Temperature distribution inside the crystal of different lengths reached at different instants during growth.

Concentration of point defects obtained here is not the actual concentration of point defects that remained in the crystal wafer. In fact, after the crystal is grown to the desired length, the crystal is cooled to room temperature without growing. So, the distribution of defects obtained here is the initial stage of the defects for rapid cooling by turning the heater off. The dynamics during the cooling in which there is no growth has to be represented by a different temperature field.

At the beginning the crystal is thin. So, almost all of its portion is in touch with the very hot melt, where most of the defects are assumed to form. So, we have taken the initial distribution inside the thin crystal as the uniform highest value equal to C_j^0, $j = I, V$. Fig. 2 shows the distribution of point defects inside the crystal at the different times during growth. During the very first time interval, the crystal being thin and hot, the point defects, which are formed at the interface, do not get sufficient time to undergo diffusion and recombination. This results in high and uniform concentration inside the thin crystal of initial stage. As the time increases, the crystal length becomes longer. This causes larger variation of point defects concentration inside the crystal. The concentration decreases from the interface to the top at each of the time instants (9 hours, 18 hours and final). Moreover, at the top of the crystal, the slope of the curves tends to zero at every instant due to no flux boundary condition. However, away from the top, slope decreases as the crystal becomes longer and longer showing that the concentration of defects falls quickly from the interface to the top at the early hours of growth and slowly at the late hours. Therefore, the middle part of the final crystal can be expected to have approximately uniform defects. We notice that the value at the top remains almost the same at 18 hours and 28 hours. While the top portion of the crystal asymptotically approaches steady state, the interface portion remains approximately steady state with the highest defect-concentration due to formation of the defects. It can be

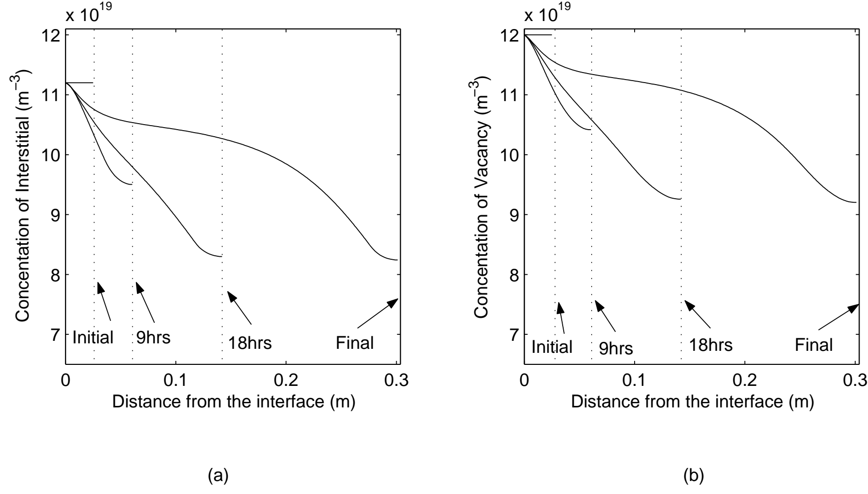

Figure 2: Distribution of (a) interstitial (b) vacancy inside the crystal of different lengths reached at different times during growth.

seen in Fig 3. The major change inside a point of the crystal takes place until it reaches a certain distance from the interface, after which it becomes almost steady-state. A rapid drop of the concentration near the interface can be interpreted as the effect of recombination. As the recombination becomes more effective at the higher temperatures, it causes the quick reduction of concentration near the interface.

Actually, how many times the concentrations are bigger than their equilibrium values determines how serious the defects are. These values are called the supersaturation of defects. According to Tiller [19], the supersaturation value can determine the size of the dislocation loops formed due to the supersaturation of vacancy and the size of the extrinsic stacking fault loops formed due to the supersaturation of interstitial. Therefore, an analysis of the supersaturation of point defects is important for the study of the defect formation. The supersaturations of interstitial and vacancy obtained inside the crystal at the different times (0 hours, 9 hours, 18 hours and 28 hours) during the growth are shown in Fig. 4. Figure shows that the supersaturation of interstitial defects is higher than that of vacancy defects even though the actual value of interstitial concentration is less. For a short crystal, the supersaturation value is small but as the length of the crystal increases the supersaturation value increases which increases the possibility of the formation of more dislocation loops. As mentioned earlier the top of the crystal is almost the steady state, where the supersaturation of interstitial defects is much more higher than that of vacancy defects. So, the top will most probably contain more interstitial type loops than vacancy-type loops.

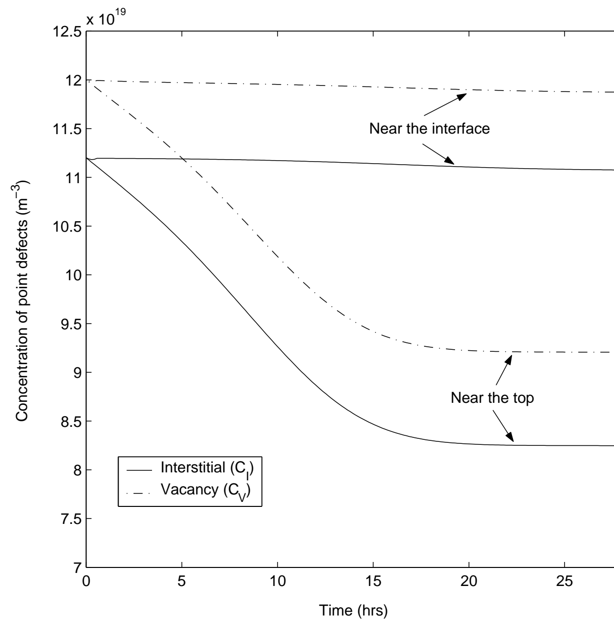

Figure 3: Change of concentration of interstitial and vacancy with respect to time near the interface and the top.

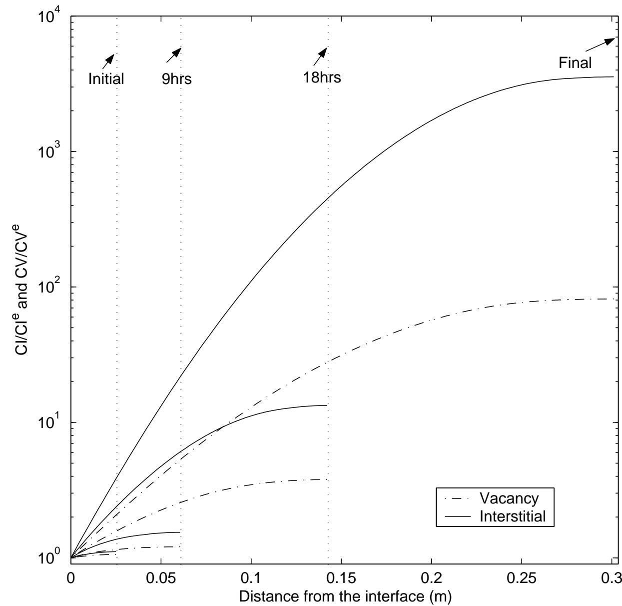

Figure 4: The concentrations of interstitial and vacancy normalized with their equilibrium value distributed inside the crystal at the different times 0 hours, 9 hours, 18 hours and 28 hours.

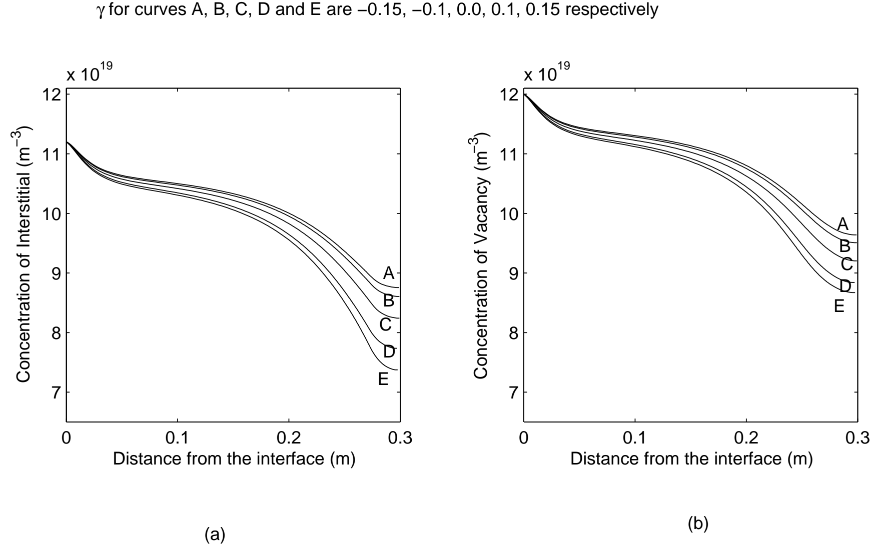

Figure 5: The concentration distribution of (a) interstitial (b) vacancy for the values of $\gamma = -0.15, -0.1, 0, 0.1, 0.15$ in the final crystal of length 30 cm.

4.1.2 Effect of the thermal fluxes

In our model together with the temperature equation, γ represents the non-dimensional heat flux from the melt and h_{gs} represents the crystal-gas heat transfer coefficient. We present a brief analysis of the dependence of point defects concentration upon the values of γ and h_{gs}. As the length of the crystal grown depends upon these values, in both cases, programs are run for different times for the different values of γ and for the different values of h_{gs} so that the final length of the crystal is 30 cm. Fig. 5 (a) and Fig. 5 (b) show the interstitial concentration distribution and the vacancy concentration distribution respectively at the end of the growth for the different values of γ. The values of γ chosen are -0.15, -0.1, 0, 0.1, 0.15. For each value of γ the value of h_{gs} is fixed as 3 W/m^{2}K. As the value of γ increases, the concentration decreases. Therefore, the higher the value of γ, the better the crystal grown. In practice, the value of γ can be controlled by adjusting the growth condition such as heater temperature, crucible shape etc. However, the value of γ can be increased only upto a certain limit otherwise the crystal will not grow.

It has been assumed that the heat transfer coefficient, h_{gs}, incorporates both convective and radiative heat transfer. We did observation of the final distribution of both interstitial and vacancy by taking different values of h_{gs}. The values of h_{gs} chosen are 1, 2, 3 and 4 W/m^{2}K. For each value of h_{gs} the value of γ is fixed as 0. Fig 6 (a) and Fig 6 (b) show the interstitial concentration distribution and vacancy concentration distribution respectively for the values 1, 2, 3 and 4 W/m^{2}K of h_{gs}. Near the interface, the concentration has negligible effect of h_{gs}. But away from the interface, the value of concentration increases with increase in the value of h_{gs}. Therefore, The better crystals can be obtained by adjusting the lower

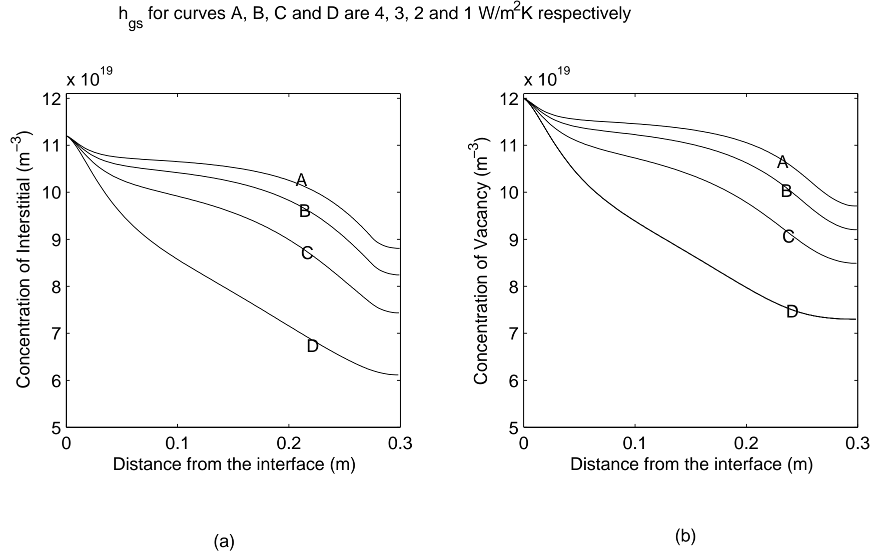

Figure 6: The concentration distribution of (a) interstitial (b) vacancy for the values of $h_{gs} = 1, 2, 3, 4 \mathrm{W/m^2K}$ in the final crystal of length 30 cm.

value of h_{gs}. This fact is consistent with Bohun et al [1] that one should try to reduce the heat flux via the lateral surface when a crystal of larger radius is grown. According to them, the heat flux through the side surface is an important factor for reducing the overall thermal stress inside the crystal.

4.2 Two-dimensional case

In the following section, we will present a brief analysis of the two-dimensional model. In this case, we take the value of $h_{gs} = 3$ W/m^{2}K and the radius of crystal $R = 3$ cm. In the simulation, a crystal is grown for 20 hours producing a crystal of 30 cm length. Here the crystal has grown faster than the previous case because of the smaller value of R.

Fig. 7 shows the distribution of point defects inside the final crystal of length 30 cm and radius 3 cm grown for 20 hours. Large variations of the concentration of both vacancy and interstitial occur in the axial direction. The variation along the radial direction is small. We can clearly see that the vacancy is the dominant defect everywhere inside the crystal.

5 Conclusion

We have presented a computational model for the distribution of point defects inside indium antimonide crystal grown by the CZ-technique. We found that the major change inside a point of the crystal takes place while it is within a certain height from the interface (i.e. up to a certain temperature), after that it becomes an almost steady-state. The middle

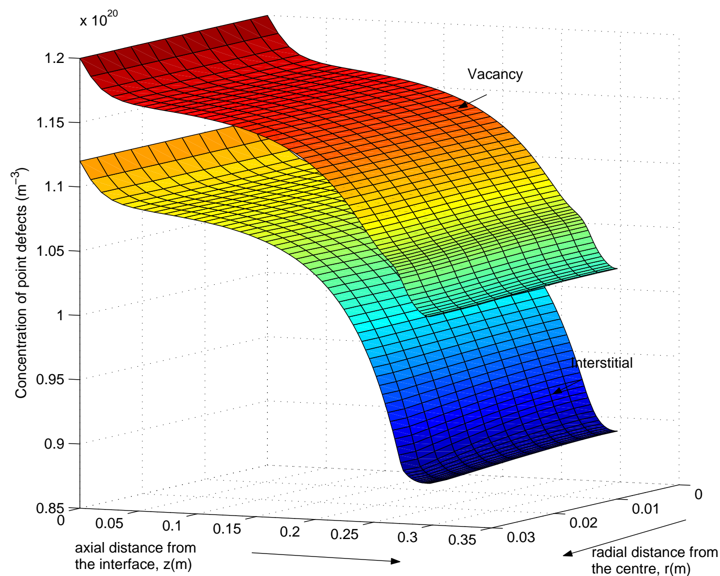

Figure 7: The point defect distribution inside the final crystal of length 30 cm.

portion of the final crystal contains approximately uniform defects. Even though the vacancy concentration is higher than the interstitial concentration, the supersaturation value of the interstitial is higher than that of the vacancy showing that the top of the final crystal most probably contains the interstitial type loops than the vacancy type loops. Based on our results, a better crystal can be grown by increasing the heat flux from the melt or/and by decreasing the lateral heat transfer coefficient. The radial variation of defects concentration is negligible compared to their axial variation.

The basic model can be extended to include more types of defects. A brief discussion of such a generalization is given in the Appendix.

Acknowledgement: The authors are very much thankful to Dr. C. Ou, Dr. C. S. Bohun and Dr. I. Frigaard for their valuable suggestions. The authors also wish to thank Firebird Semiconductor Inc. and the Mathematics for Information Technology and Complex System (MITACS) for their financial support.

References

[1] C.S. Bohun, I. Frigaard, H. Huang and S. Liang, A Perturbation Model for the Growth of Type III-V Crystal, submitted (2005).

[2] F.H. Eisen and C.E. Birchenall, Self-Diffusion in Indium Antimonide and Gallium Antimonide, *Acta Metallurgica*, **5**, pp. 265-274 (1957).

[3] N.N. Greensood, Ionic Crystals Lattice Defects and Nonstoicheometry. Butterworth and Co. Ltd., London (1968).

[4] R. Habu, T. Iwasaki, H. Harada and A. Tomiura, *japanese Journal of Applied Physics*, **33**, 1234 (1994).

[5] R. Habu, A. Tomiura, *Japanese Journal of applied Physics*, **35**, 1 (1996).

[6] D.T.J. Hurle, Handbook of Crystal Growth. Amsterdam, New York, North Holand (1993).

[7] D.L. Kendall and R.A. Huggins, Self-Diffusion in Indium Antimonide, *Journal of Applied Physics* **40** (no.7), pp. 2750-2759 (1969).

[8] T. L. Larsen et al, Numerical Simulation of Point Defect Transport in Floating-zone Silicon Single Crystal Growth, *Journal of Crystal Growth*, **230**, pp 300-304 (2001).

[9] M. Ma et al, Relationship between Characteristics of Defects in CZ-Si Crystals and V/G Ratios by Multi-chroic Infrared Light Scattering Tomography, *Journal of Crystal Growth*, **234**, pp 296-304 (2002).

[10] K. Nakamura, T. Saishoji and J. Tomioka, Grown-in Defects in Silicon Crystals, *Journal of Crystal Growth*, **237-239**, pp. 1678-1684 (2002).

[11] K. Nakamura, T. Saishoji and J. Tomioka, Simulation of Point Defect Distributions in Silicon Crystals During Melt-growth, *Journal of Crystal Growth* **237-239**, pp. 1678-1684 (2000).

[12] K. Nakamura et al., Formation of Process of Grown-in Defects in Czchralski Grown Silicon Crystal, *Journal of Crystal Growth*, **180**, pp. 61-72 (1997).

[13] T. Okino, Intrinsic Point Defects and Grown-in Defects in Silicon, *Solid State Phenomena* **71**, pp 1-22 (2000).

[14] M. Okui and M. Nishomoto, *Journal of Crystal Growth* **237-239**, pp 1651-1656 (2002).

[15] N. Puzanov, A. Eidenzon, D. Puzanov, Modeling Microdefect Distribution in Dislocation Free Si-Crystals Grown from the Melt, *Journal of Crystal Growth* **179**, pp 468-478 (1997).

[16] A. Rastogi and K. Reddy, Self-diffusion in Polycrystalline InSb Films, IOP Publishing Ltd., pp. 2067-2072 (1994).

[17] T. Sinno et al., Defect Engineering of Czochralski Single-crystal Silicon, *Material Science and Engineering* **28**, pp. 149-198 (2000).

[18] W.A. Tiller, Grown-in Point Defects in Microscopic Defect Formation in CZ Silicon I. The One-dimensional, Steady-state Approximation, *Journal of Crystal Growth* **186**, pp. 113-127 (1998).

[19] W.A. Tiller, The Science of Crystallization. Cambridge University Press, Cambridge, New York, Port Chester, Melbourne, Sydney (1991).

[20] N. Vaidya, Modeling Grown-In Defects in Indium Antimonide Crystal, M. Sc Thesis, York University (2004).

[21] V.V. Voronkov and R. Falster, Vacancy and Self-interstitial Concentration Incorporated into Growing Silicon Crystal, *Journal of Applied Physics* **86** (11) pp. 5975-5982 (1999).

[22] V.V. Voronkov, The Mechanism of Swirl Defects Formation in Silicon, *Journal of Crystal Growth* **59** pp. 625-643 (1982).

[23] H.U. Walter, Generation and Propagation of Defects in Indium Antimonide. *J. Electrochem. Soc.: Solid-State Science and Technology* **124** (2), pp. 250-258 (1977).

6 Appendix: A Model with More Defects Types

The basic model presented in this paper can be extended to include more defects types, which is outlined here. Indium antimonide, being a compound semiconductor, can posses two types of vacancy, namely indium vacancy and antimony vacancy; and two types of interstitial, namely indium interstitial and antimony interstitial. We neglect the impurity atom, interstitialcy defects and charged species. Therefore, we propose the model which governs the dynamics of four types of point defects, namely indium interstitial, antimony interstitial, indium vacancy and antimony vacancy.

As there are two types of interstitials and two types of vacancies, there are four possible ways of recombination. Taking the recombination into account along with all those considered in early sections of this paper, we will have model equations as follows:

$$\frac{\partial C_j}{\partial t} = \nabla \cdot (D_j \nabla C_j - \vec{f}_p C_j) - \sum_m R_{jm}(C_j C_m - C_j^e C_m^e), \tag{23}$$

where C_j = volume concentrations of $j = I_i$ (indium interstitial), I_s (antimony interstitial), V_i (indium vacancy), V_s (antimony vacancy). Here, $m = V_i, V_s$ if $j = I_i$ or I_s and $m = I_i$, I_s if $j = V_i$ or V_s. Formula for reaction rate R_{jm} of recombination between j-type of interstitial (or vacancy) and m-type of vacancy (or interstitial) is similar to the previous case. Detail analysis of this model can be found in [20].